Inorganic Chemistry

Article

pubs.acs.org/IC

Uranyl-Promoted Peroxide Generation: Synthesis and Characterization of Three Uranyl Peroxo $[(UO_2)_2(O_2)]$ Complexes

Sonia G. Thangavelu and Christopher L. Cahill*

Department of Chemistry, The George Washington University, 800 22nd Street, NW, Washington, DC 20052, United States

Supporting Information

ABSTRACT: Three novel uranyl(VI) peroxide complexes, $[(UO_2)_2(CH_3COO)_2(O_2)(C_{10}H_8N_2)]$ (**1**), $[(UO_2)_2(CH_3COO)_2(O_2)(C_{12}H_{12}N_2)]$ (**2**), and $[(UO_2)_3(CH_3COO)_4(O_2)(C_{15}H_{11}N_3)_2]$ (**3**), have been synthesized and characterized by single-crystal X-ray diffraction, powder X-ray diffraction, and luminescence spectroscopy. Each of these structures feature a $[(UO_2)_2(O_2)]$ dimer with additional coordination by acetate, 2,2′-bipyridine (BPY), 5,5′-dimethyl-2,2′-bipyridine (MeBPY), or 2,2′:6,2″-terpyridine (TPY). Compound **3** consists of an additional uranyl unit functionalized with a TPY donor ligand. The presence of the peroxo ligand in **1**−**3** is due to in situ generation of peroxide when preparative solutions of **1**−**3** were exposed to ambient light and/or sunlight.

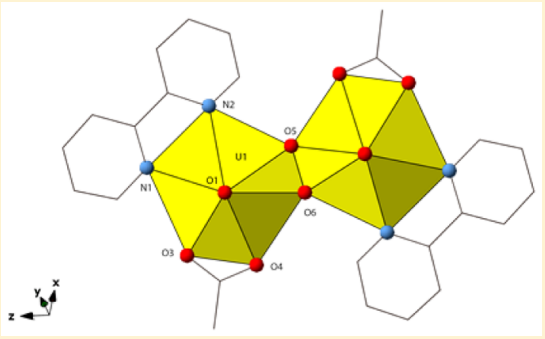

INTRODUCTION

Uranyl peroxide materials have received much attention due to their relevance to the nuclear fuel cycle, particularly as alteration products of used nuclear fuel. For example, the minerals studtite $[(UO_2)(O_2)(H_2O)_2{\cdot}2H_2O]$ and meta-studtite $[(UO_2)(O_2){\cdot}2H_2O]$ have been reported to form when peroxide is generated via α-radiolysis of water during dissolution of spent nuclear fuel under aqueous conditions.[1−6]

Uranyl materials containing peroxo ligands are often synthesized readily using H_2O_2 as a reagent. Studtite may be prepared straightforwardly by reacting H_2O_2 with uranyl in acidic media, and uranyl triperoxide salts have been crystallized from alkaline or alcohol solutions in order to gain insights into U(VI) peroxide speciation.[7−11] Perhaps more interesting, however, is the rich and extensive family of UO_2^{2+} peroxo nanoclusters prepared by Burns and co-workers.[1] The structures of these materials resemble C_{60} fullerenes and often incorporate differently sized anions such as nitrate, oxalate, or phosphate.[1,6,12] A general structural theme is that peroxide anions serve to bridge between two uranyl centers that overall exhibit either pentagonal or hexagonal bipyramidal geometries. Beyond structural interests, however, understanding the formation of peroxo materials in the arena of used nuclear fuel may be useful in terms of environmental models for possible actinide transport or mass-based separations during fuel reprocessing.[13,14]

Uranyl peroxide materials have also been prepared without utilizing hydrogen peroxide as an added reagent in synthetic procedures.[15−18] Several reports of the in situ generation of peroxide have suggested photoexcitation of UO_2^{2+} in solution is the cause for the observed uranyl peroxide complexes. Specifically, when UO_2^{2+} is exposed to light, the excited $^*UO_2^{2+}$ ion is generated. This ion is subsequently reduced by electron abstraction from H_2O or an organic substrate to produce UO_2^+. Consequently, the UO_2^+ species can then be reoxidized by atmospheric dioxygen to regenerate UO_2^{2+} and yield H_2O_2 as a byproduct, which in turn may coordinate to UO_2^{2+} to make uranyl peroxide materials.[16−18] This mechanism has been proposed to account for the photocatalytic properties of UO_2^{2+} in which examples of UO_2^{2+} hybrid assemblies or mesoporous supported UO_2^{2+}-silicates have shown to oxidize various organic substrates.[19−23] More recently, an alternative mechanism has been proposed by McGrail and co-workers, in which they suggest that formation of uranyl peroxide complexes is due to the loss of dihydrogen from a water- or hydroxo-bridged diuranyl intermediate.[24]

A number of uranyl peroxide materials have been synthesized with N-donor ligands such as 2,2′-bipyridine (BPY), 5,5′-dimethyl-2,2′-bipyridine (MeBPY), and 2,2′:6,2″-terpyridine (TPY).[25−30] Our own interest in these ligands was demonstrated in a previous study wherein we explored the TPY ligand as a means of affecting UO_2^{2+} speciation and directing the formation of hybrid materials with unhydrolyzed monomeric UO_2^{2+} centers. There, different O-donor linkers were used to assemble uranyl-TPY complexes into binuclear "pseudo dimers" and, in turn, explore the effect on uranyl emission.[31] We noted that the presence of certain O-donor ligands (e.g., NDC) effectively quenched uranyl emission,[31] whereas the extent of π-stacking between TPY[32] or 2,6-PYDC (pyridine 2,6-dicarboxylic acid)[33] units may influence the observed range of uranyl emission. As such, we attempted to synthesize N-donor "end members" in the absence of O-donors in order to explore their luminescence and thus eliminate the influence of O-

Received: November 19, 2014
Published: April 15, 2015

DOI: 10.1021/ic502767k
Inorg. Chem. 2015, 54, 4208−4221

Table 1. Synthetic Conditions and Molar Ratios for Compounds 1−3

	1	2	3
formula	$[(UO_2)_2(CH_3COO)_2(O_2)(C_{10}H_8N_2)]$	$[(UO_2)_2(CH_3COO)_2(O_2)(C_{12}H_{12}N_2)]$	$[(UO_2)_3(CH_3COO)_4(O_2)\ (C_{15}H_{11}N_3)_2]$
method	A	A*, B, B*, B**	A
metal (mg, mmol)	$UO_2(CH_3COO)_2{\cdot}2H_2O$ (30 mg, 0.070 mmol)	$UO_2(CH_3COO)_2{\cdot}2H_2O$ (30 mg, 0.070 mmol)	$UO_2(CH_3COO)_2{\cdot}2H_2O$ (30 mg, 0.070 mmol)
ligand (mg, mmol)	BPY(10.9 mg, 0.070 mmol)	MeBPY (12.9 mg, 0.070 mmol)	TPY (16.9 mg, 0.070 mmol)
solvent (mL)	MeOH (3 mL)	1:1 MeOH−acetone (3 mL) or MeOH alone (3 mL)	MeOH (3 mL)
crystals?	yes, yellow block crystals	yes, yellow block crystals	yes, orange block crystals
pure?	yes	yes	yes

Table 2. Synthetic Conditions and Molar Ratios for the Control Experiments of 1−3

	1	2	3
formula	$[(UO_2)_2(CH_3COO)_2(O_2)(C_{10}H_8N_2)]$	$[(UO_2)_2(CH_3COO)_2(O_2)(C_{12}H_{12}N_2)]$	$[(UO_2)_3(CH_3COO)_4(O_2)(C_{15}H_{11}N_3)_2]$
method	D	E	D
metal (mg, mmol)	$UO_2(CH_3COO)_2{\cdot}2H_2O$ (30 mg, 0.070 mmol)	$UO_2(CH_3COO)_2{\cdot}2H_2O$ (30 mg, 0.070 mmol)	$UO_2(CH_3COO)_2{\cdot}2H_2O$ (30 mg, 0.070 mmol)
ligand (mg, mmol)	BPY(10.9 mg, 0.070 mmol)	MeBPY (12.9 mg, 0.070 mmol)	TPY (16.9 mg, 0.070 mmol)
solvent (mL)	MeOH (3 mL)	1:1 MeOH−acetone (3 mL)	MeOH (3 mL)
crystals?	no, yellow solution	no, yellow solid	no, yellow solid
peroxo phase?	no	no	no

donors since uranyl complexes containing TPY- or BPY-like ligands are known to affect UO_2^{2+} emission.[34,35] The syntheses of end members under hydrothermal conditions proved unsuccessful, and we therefore decided to explore room-temperature self-assembly. Somewhat unexpectedly, we found that room-temperature synthesis conditions led to the formation of uranyl peroxo complexes in the presence of either sunlight or ambient (laboratory) light. Moreover, an extensive experimental effort was undertaken to confirm reproducibility and exact reaction conditions required for peroxo formation and subsequent crystallization. We herein report the synthesis, crystal structures, and luminescence properties of three novel N-donor uranyl(VI) peroxide acetate complexes using BPY, MeBPY, and TPY: $[(UO_2)_2(CH_3COO)_2(O_2)(C_{10}H_8N_2)]$ (**1**), $[(UO_2)_2(CH_3COO)_2(O_2)(C_{12}H_{12}N_2)]$ (**2**), and $[(UO_2)_3(CH_3COO)_4(O_2)(C_{15}H_{11}N_3)_2]$ (**3**) respectively.

EXPERIMENTAL SECTION

Caution! *$UO_2(CH_3COO)_2{\cdot}2H_2O$ (Fisher Scientific) contains depleted uranium. Handling and storage of toxic and radioactive substances should be followed using appropriate protocols.*

General Synthesis of Compounds 1−3. The ligands BPY, MeBPY, and TPY were purchased from VWR and used as received. Compounds **1**−**3** were prepared using three distinct methods: sunlight (A), heating (B), and sunlight/heating (B*). The sunlight method (A) is as follows: a mixture of $UO_2(CH_3COO)_2{\cdot}2H_2O$ (30 mg, 0.070 mmol, 1 equiv) and N-donor ligand (0.070 mmol, 1 equiv) was added to MeOH (3 mL) in a 25 mL scintillation vial. The vial was then placed on a windowsill exposed to sunlight for 7 days; block crystals appeared after a few days. The heating method (B) is as follows: A mixture of $UO_2(CH_3COO)_2{\cdot}2H_2O$ (30 mg, 0.070 mmol, 1 equiv) and N-donor ligand (0.070 mmol, 1 equiv) was added to a 3 mL solution of acetone−MeOH (1:1) in a 25 mL scintillation vial. The vial was then heated in an oil bath at 50 °C for 24 h while exposed to ambient light. Block crystals were observed after cooling the vial to room temperature overnight. The sunlight/heat method (B*) is as follows: A mixture of $UO_2(CH_3COO)_2{\cdot}2H_2O$ (30 mg, 0.070 mmol, 1 equiv) and N-donor ligand (0.070 mmol, 1 equiv) was added to a 3 mL solution of acetone−MeOH (1:1) in a 25 mL scintillation vial. The vial was then heated in an oil bath at 50 °C for 24 h while exposed to ambient light. After heating, this vial was then placed on a windowsill exposed to sunlight for 7 days in which block crystals were observed after a few days. The synthetic methods and molar ratios employed for **1**−**3** can be found in Table 1.

Our attempts to synthesize compound **2** using method A was unsuccessful due to the insolubility of MeBPY in methanol alone, thus requiring the addition of acetone and heat (methods B and B*). To determine whether compound **2** could form independent of heat, a modified sunlight method (A*) was employed. In method A*, the molar ratios of MeBPY and uranyl acetate outlined in Table 1 were added to a 3 mL 1:1 MeOH−acetone solution in a 25 mL scintillation vial. This vial was placed on a windowsill exposed to sunlight for 7 days. After this time period, crystals were not observed; thus the yellow solution was allowed to slowly evaporate, in which yellow block crystals were observed after a few days. The unit cells of differently sized crystals with different crystal morphologies (e.g., blocks and needles) were collected at 100 K in which the cell parameters of each crystal matched the unit cell of **2**, although the powder X-ray diffraction (PXRD) pattern of the products from method A* does not seem to be a conclusive match to compound **2** (see Supporting Information Figure S4). These results (despite the observed PXRD) suggest that compound **2** can form independent of heat if acetone is added to solubilize MeBPY. To determine whether compound **2** could also form independent of the use of acetone, a modified sunlight/heating method (B**) was performed. In method B**, the molar ratios of MeBPY and uranyl acetate outlined in Table 1 were added to a 3 mL MeOH solution in a 25 mL scintillation vial. This vial was then placed in an oil bath and allowed to heat at 50 °C while exposed to ambient light. The vial was then placed on a windowsill exposed to sunlight for 7 days. Yellow block crystals were observed after a few days. Products from method B** were indicative of **2** (see Supporting Information Figure S5), suggesting that compound **2** can also form when a methanol solution is heated in the absence of acetone.

Efforts to synthesize **1** and **3** using method B were also performed. The PXRD patterns for **1** and **3** using both methods A and B were compared. The products from heating method B for **1** and **3** were not indicative of the peroxo phase and remain unidentified (see Supporting Information Figures S6, S7).

As our control experiments, the syntheses of **1**−**3** were attempted in the absence of light (ambient or sun) following two synthetic methods: dark (D) and heating/dark (E). The dark method (D) is as follows: a mixture of $UO_2(CH_3COO)_2{\cdot}2H_2O$ (30 mg, 0.070 mmol, 1 equiv) and N-donor ligand (0.070 mmol, 1 equiv) was added to MeOH (3 mL) in a 25 mL scintillation vial. The vial was then wrapped with aluminum foil and placed in a drawer without exposure to light

DOI: 10.1021/ic502767k
Inorg. Chem. 2015, 54, 4208−4221

Table 3. Synthetic Conditions and Molar Ratios for the Solvothermal Experiments of 1−3

	1	2	3
formula	$[(UO_2)_2(CH_3COO)_2(O_2)(C_{10}H_8N_2)]$	$[(UO_2)_2(CH_3COO)_2(O_2)(C_{12}H_{12}N_2)]$	$[(UO_2)_3(CH_3COO)_4(O_2)\ (C_{15}H_{11}N_3)_2]$
metal (mg, mmol)	$UO_2(CH_3COO)_2{\cdot}2H_2O$ (30 mg, 0.070 mmol)	$UO_2(CH_3COO)_2{\cdot}2H_2O$ (30 mg, 0.070 mmol)	$UO_2(CH_3COO)_2{\cdot}2H_2O$ (30 mg, 0.070 mmol)
ligand (mg, mmol)	BPY(10.9 mg, 0.070 mmol)	MeBPY (12.9 mg, 0.070 mmol)	TPY (16.9 mg, 0.070 mmol)
solvent (mL)	MeOH (3 mL)	1:1 MeOH−acetone (3 mL)	MeOH (3 mL)
temperature (°C)	120	120	120
number of days	5	5	5
crystals?	no, gray-green solid	no, yellow solid	no, orange solid
peroxo phase?	no	no	no

Table 4. Crystallographic Data for Compounds 1−3

	1	2	3
Formula	$[(UO_2)_2(CH_3COO)_2(O_2)(C_{10}H_8N_2)]$	$[(UO_2)_2(CH_3COO)_2(O_2)(C_{12}H_{12}N_2)]$	$[(UO_2)_3(CH_3COO)_4(O_2)(C_{15}H_{11}N_3)_2]$
fw	1002.51	1058.62	1544.80
temperature	100 K	100 K	100 K
wavelength	0.710 73 Å	0.710 73 Å	0.710 73 Å
cryst system	orthorhombic	monoclinic	triclinic
space group	*Pbca*	$P2_1/n$	$P\bar{1}$
unit cell dimens	a = 11.5190(13) Å	a = 10.1075(5) Å	a = 11.6277(12) Å
	b = 13.4899(16) Å	b = 19.0863(9) Å	b = 13.3121(14) Å
	c = 16.7373(19) Å	c = 16.2506(7) Å	c = 15.1435(15) Å
	$\alpha = \beta = \gamma = 90°$	β = 103.1950(10)°	α = 67.522(2)°
			β = 86.610(2)°
			γ = 80.255(2)°
volume	2600.8(5) Å^3	3052.2(2) Å^3	2134.7(4) Å^3
Z	4	4	2
density (calcd)	2.560 Mg/m^3	2.304 Mg/m^3	2.403 Mg/m^3
absorp coeff	12.503 mm^{-1}	10.660 mm^{-1}	11.430 mm^{-1}
reflns collected	37 050	44 974	31 899
indep reflns	3822 [R(int) = 0.0473]	8747 [R(int) = 0.0512]	11 869 [R(int) = 0.0543]
final R indices [$I > 2\sigma(I)$]	R_1 = 0.0333, wR_2 = 0.0755	R_1 = 0.0286, wR_2 = 0.0508	R_1 = 0.0484, wR_2 = 0.1031

(ambient or sun) for 7 days. Yellow solids or solutions were observed after a few days. The heating/dark method (E) is as follows: A mixture of $UO_2(CH_3COO)_2{\cdot}2H_2O$ (30 mg, 0.070 mmol, 1 equiv) and N-donor ligand (0.070 mmol, 1 equiv) was added to a 3 mL solution of acetone−MeOH (1:1) in a 25 mL scintillation vial. The vial was then wrapped with aluminum foil and heated in an oil bath at 50 °C for 24 h. After cooling to room temperature, this vial was then placed in a drawer without exposure to light (ambient or sunlight) for 7 days; a yellow solid appeared after a few days. The synthetic conditions and molar ratios for the attempted syntheses of **1**−**3** using methods D and E can be found in Table 2.

The products from methods D and E were compared to the calculated PXRD patterns of **2** and **3** and were not indicative of the peroxo phase (see Supporting Information Figures S9, S10). Attempts to identify the bulk via comparisons of the observed PXRD patterns to studtite (calculated from ref 3) and uranium oxide phases were unsuccessful. A description of phase identification of the bulk can be found in the Supporting Information.

The syntheses of **1**−**3** were also attempted with the addition of 30% H_2O_2 using methods D and E to determine whether **1**−**3** could also form independent of sunlight using hydrogen peroxide exclusively. The synthesis of each compound uses the same conditions as seen in Table 2 but with the addition of 0.1 mL of 30% H_2O_2. However, products from these methods were not indicative of **1**−**3** and remain unidentified (see Supporting Information Figures S11−S13).

The syntheses of **1**−**3** were also attempted under solvothermal conditions as follows: in a 25 mL Teflon-lined cup, the reagents $UO_2(CH_3COO)_2{\cdot}2H_2O$ (30 mg, 0.070 mmol, 1 equiv) and N-donor ligand (0.070 mmol, 1 equiv) were added to a solution of MeOH or a 1:1 MeOH−acetone mixture (3 mL). The Teflon cup was then placed in a stainless steel Parr bomb and heated statically at 120 °C for 5 days. The Parr bomb was then allowed to cool slowly overnight. Solids were isolated from the mother liquor, washed with MeOH, and allowed to air-dry. The PXRD patterns of the solids from these experiments were not indicative of **1**−**3** (see Supporting Information Figures S14−S16) and remain unidentified. A summary of the synthetic conditions and molar ratios for the attempted syntheses of **1**−**3** via solvothermal conditions can be found in Table 3 as well as in the Supporting Information (Figure S30).

Crystal Structure Determination. Single crystals isolated from each bulk sample were mounted on MiTeGen micromounts. Reflections were collected using 0.5° φ and ω scans on a Bruker SMART diffractometer equipped with an APEX II CCD detector using Mo Kα radiation at 100 and 298 K. All data were integrated using the SAINT software package, and an absorption correction was applied using SADABS. Structures were determined using direct methods (either SIR-92 or SHELXS-2013) and then refined using SHELXL-2013 within the WinGX software package,[36−38] in which all the non-hydrogen atoms were refined anisotropically. Hydrogen atoms residing on the carbon atoms of BPY, MeBPY, and TPY ligands were placed in calculated positions and allowed to ride on their parent atoms. Tests for additional symmetry in all structures were done using PLATON.[39]

For compound **1**, disorder about the peroxo and axial oxygen atoms O5 and O2, respectively, were observed at room temperature. This required a PART command in which the oxygen atoms were modeled and refined successfully. A low-temperature data collection of **1** was also performed in an attempt to restrict the thermal motions of the parent atoms and thus potentially resolve the disorder seen at room temperature. Disorder of the axial oxygen atom was not observed at low temperature, yet the disorder about the peroxo oxygen atom persisted, thus requiring a PART command. Compounds **2** and **3** were

DOI: 10.1021/ic502767k
Inorg. Chem. 2015, 54, 4208−4221

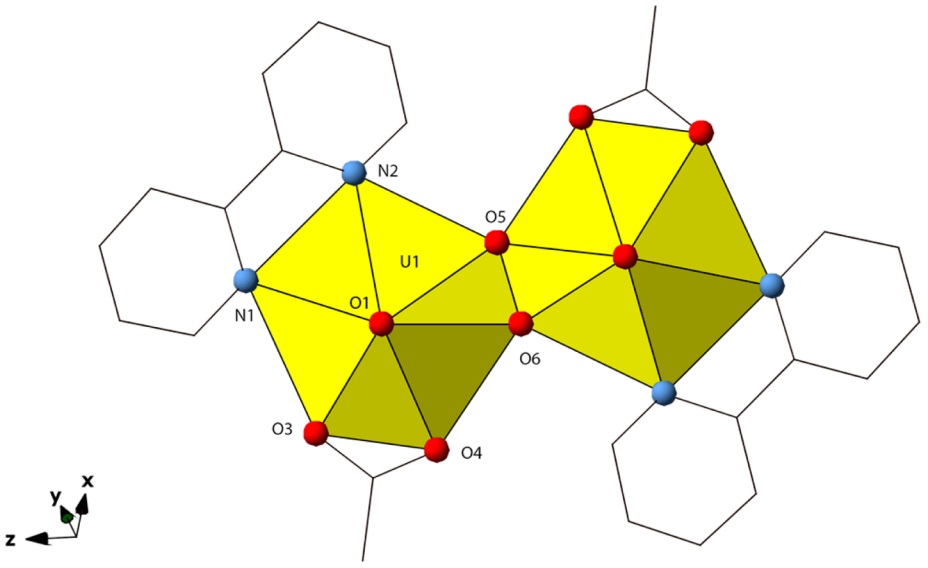

Figure 1. Local structure of **1**. Spheres represent nitrogen (blue) and oxygen (red) atoms. Yellow polyhedra represent uranium.

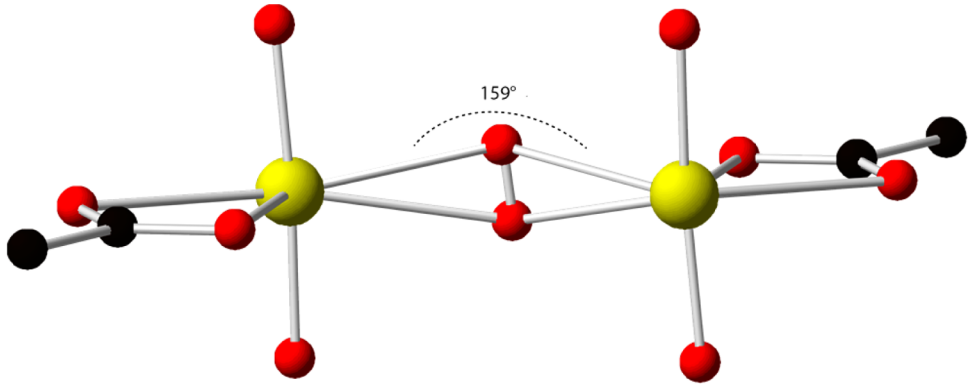

Figure 2. Ball-and-stick representation of **1** showing the U−O_2−U dihedral angle. This angle was measured from the center of U1 to the midpoint of the O5−O6 bond and the center of U1′. BPY ligands are omitted for clarity.

also collected at low temperature, yet disorder of the hydrogen atoms present on the methyl carbon atom C17 was observed in **3**. This required an AFIX 123 command to idealize the disordered methyl hydrogen atoms to two sets of methyl hydrogen conformations in which each conformation is rotated from each other by 60°. Crystallographic Information Files (CIFs) of compounds **1**−**3** at 298 and 100 K were deposited at the Cambridge Crystallographic Data Centre (CCDC) and can be obtained via http://www.ccdc.cam.ac.uk by citing deposition numbers 1026946 (**1**, 100 K), 1026947 (**2**, 100 K), 1026948 (**3**, 100 K), 1026949 (**1**, 298 K), 1026950 (**2**, 298 K), and 1026951 (**3**, 298 K). A summary of the crystallographic data for **1**−**3** obtained at 100 K can be found in Table 4. The bond lengths and angles tables for **1**−**3** along with their ORTEP representations can be found in the Supporting Information (Tables S1−S3 and Figures S18−S20).

Powder X-ray Diffraction. Diffraction patterns of compounds **1**−**3** were obtained on a Rigaku MiniFlex II desktop powder X-ray diffractometer (Cu Kα, 3−60°) and analyzed using the JADE software package. Purity (or lack thereof) of bulk samples for **1**−**3** was determined by comparing observed and calculated PXRD patterns. These patterns can be found in the Supporting Information (Figures S1−S16).

Fluorescence Measurements. Compounds **1**−**3**, uranyl acetate, and ligands were crushed to fine powders using a mortar and pestle and were placed between two glass slides. Spectra were collected at 298 K (excitation: 365 or 420 nm; see Supporting Information Figure S26) using the face forward setting (45°) on a Horiba JobinYvon Fluorolog spectrophotometer, and the excitation and emission slit widths were set between 2 and 3 nm, respectively. Fluorescence spectra of the ligands and uranyl acetate were collected at room temperature (excitation: 365 nm), which can be found in the Supporting Information (Figures S22−S25). Low-temperature (77 K) fluorescence of **1**−**3** was obtained by placing several milligrams of each sample into a NMR tube, which was then submerged in a liquid nitrogen dewar assembly attached to the Fluorolog spectrophotometer. Spectra were collected using the face forward setting (45°), and the slit widths were changed to 5 nm in order to obtain suitable spectra (excitation: 365 nm) at 77 K. The low emission intensities in **1**−**3** at 77 K are qualitatively different from those obtained at 298 K. Moreover, different methods of sample preparation (e.g., NMR tube vs glass slides) at different temperatures were done in order to collect spectra. Therefore, we offer no quantitative discussions on peak intensities.

FT-IR Measurements. Solid-state spectra of **1**−**3** were collected on a PerkinElmer Frontier FT-IR spectrometer equipped with an ATR sampling accessory. Spectra were recorded at room temperature between 4000 and 600 cm^{-1}. These spectra can be found in the Supporting Information (Figures S27−S29).

RESULTS AND DISCUSSION

Structural Descriptions. *Crystal Structure of* $[(UO_2)_2(CH_3COO)_2(O_2)(C_{10}H_8N_2)]$ ***(1).*** The structure of **1** contains a $[(UO_2)_2(O_2)]$ dimer made up from a single

DOI: 10.1021/ic502767k
Inorg. Chem. 2015, 54, 4208−4221

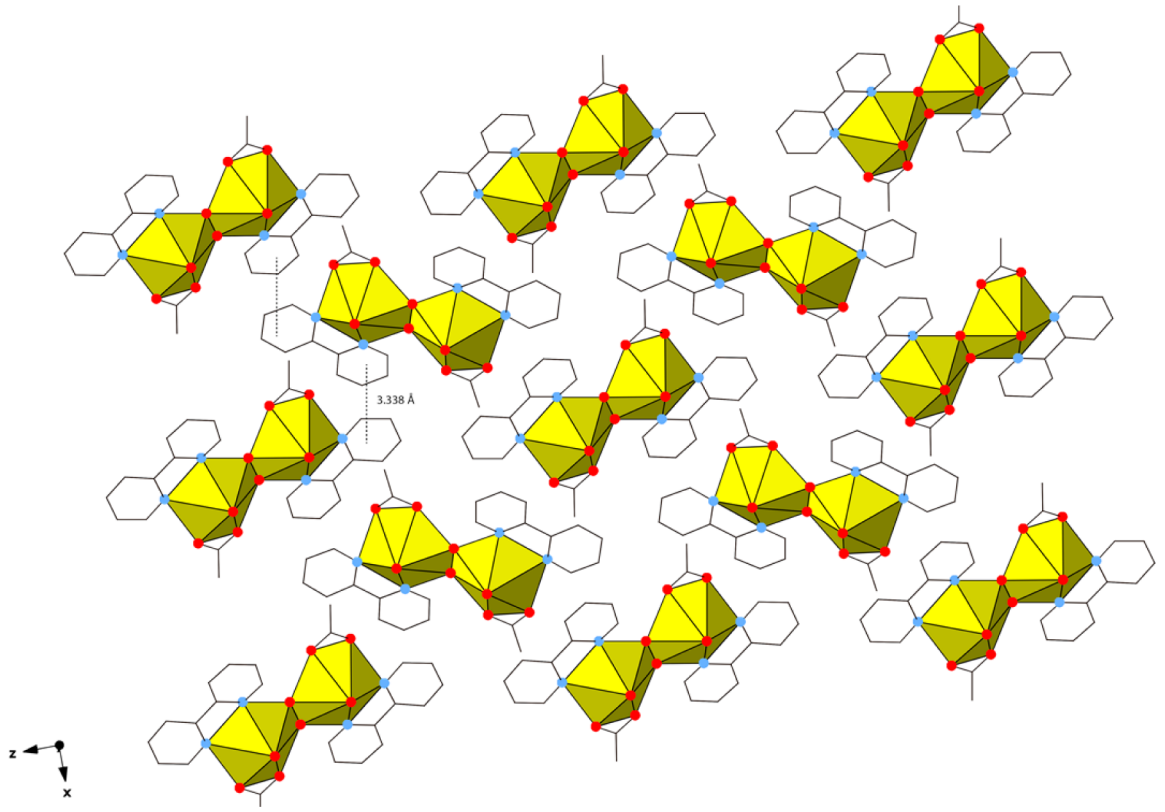

Figure 3. Packing of **1** showing $\pi-\pi$ interactions of the pyridyl rings between adjacent BPY uranyl peroxide complexes.

crystallographically unique uranyl cation (U1, O1, O2) and its symmetry equivalent as generated through an inversion center (Figure 1). U1 is bound by one bidentate BPY via N1 (2.598(4) Å) and N2 (2.640(3) Å), a bidentate acetate via O3 (2.462(3) Å) and O4 (2.470(5) Å), and a bidentate peroxide O5 (2.370(2) Å) and O6 (2.380(1) Å) (O5−O6 1.490(2) Å) to result in a hexagonal bipyramidal building unit. U1′ edge-shares with U1 via the peroxide ion to result in the $[(UO_2)_2(O_2)]$ dimer. The U1−O_2−U1′ dihedral angle within the dimer is 159° and was measured using Mercury (version 2.3)[40] by selecting two uranyl centers and the centroid of the O−O molecule (Figure 2 and Supporting Information Figure S21). The $[(UO_2)_2(O_2)]$ dimers interact with each other through $\pi-\pi$ interactions (ring centroid−centroid distance, 3.338(8) Å) between the BPY ligands to generate sheets in the (010) plane as seen in Figure 3.

Interestingly, we note that the crystal structure of the nitrate analogue of **1** ($[(UO_2)_2(NO_3)_2(O_2)(C_{10}H_8N_2)]$, Figure 4) has been reported.[25] This structure, henceforth referred to as **1n**, was compared to **1** in order to determine the influence of acetate or nitrate on the U−O_2−U dihedral angle. Compound **1n** consists of the $[(UO_2)_2(O_2)]$ dimer as **1**, yet contains the nitrate anion in place of acetate and crystallizes in a triclinic cell ($P\bar{1}$) as opposed to orthorhombic *Pbca* in **1**. The U−O_2−U dihedral angle of 180° in **1n** (Figure 4) differs from **1** (159°), which suggests that nitrate and acetate ligands influence the bond angle. The packing of **1n** includes $\pi-\pi$ interactions of the pyridyl rings (ring centroid−centroid distances: 3.758, 4.333 Å) of adjacent BPY ligands to generate sheets in the (100) plane (Figure 4), in which the π-stacking distances are larger in **1n** than **1**. In sum, the structures of **1** and **1n** are similar, yet with slight differences in the packing.

Crystal Structure of $[(UO_2)_2(CH_3COO)_2(O_2)(C_{12}H_{12}N_2)]$ (**2**). The structure of **2** contains a $[(UO_2)_2(O_2)]$ dimer made up from two crystallographically unique uranyl cations (U1, O1, O2 and U2, O7, O8) as seen in Figure 5. U1 is bound by one bidentate MeBPY via N1 (2.596(3) Å) and N2 (2.639(3) Å), a bidentate acetate via O3 (2.455(3) Å) and O4 (2.457(3) Å), and a bidentate peroxide O5 (2.308(3) Å) and O6 (2.317(3) Å) (O4−O5 1.482(4) Å) to result in a hexagonal bipyramidal building unit. U2 edge-shares with U1 via the peroxide ion to result in the $[(UO_2)_2(O_2)]$ dimer. These dimers interact with each other through $\pi-\pi$ interactions (ring centroid−centroid distance, 3.652(12) Å) between the MeBPY ligands to generate sheets in the (001) plane as seen in Figure 6. Interestingly, the π-stacking distances within **1** and **2** differ slightly, with those in **2** being slightly longer compared to **1** (3.338(8) Å), perhaps due to the presence of the methyl groups. Upon closer inspection of **2**, the U1−O_2−U2 dihedral angle is 151°, which is smaller than **1** (159°).

We also note that the crystal structure of the nitrate analogue of **2** $[(UO_2)_2(NO_3)(O_2)(C_{12}H_{12}N_2)]$ has been reported and is shown in Figure 7.[30] This structure (referred to herein as **2n**) was compared to **2** for the same reasons as established for **1**. Compounds **2** and **2n** both consist of the $[(UO_2)_2(O_2)]$ dimer and crystallize in a monoclinic cell ($P2_1/n$). Interestingly, the U−O_2−U dihedral angle in **2n** is 180° (like **1n**), yet this angle is 151° in **2**. To account for this observation, the CH_3−CH_3 distances within MeBPY and the acetate of **2** were compared to the O−CH_3 distances within MeBPY and **2n** (Figure 7). The distances in **2** (~4.0 and 4.4 Å) are larger than those in **2n** (3.6 Å), suggesting that steric hindrance by the methyl groups allows for the U−O_2−U bond angle to deviate significantly from 180°. The packing of **2n** is similar to that of **2**, in which the π-stacking ring centroid−centroid distances (3.627 Å)

DOI: 10.1021/ic502767k
Inorg. Chem. 2015, 54, 4208−4221

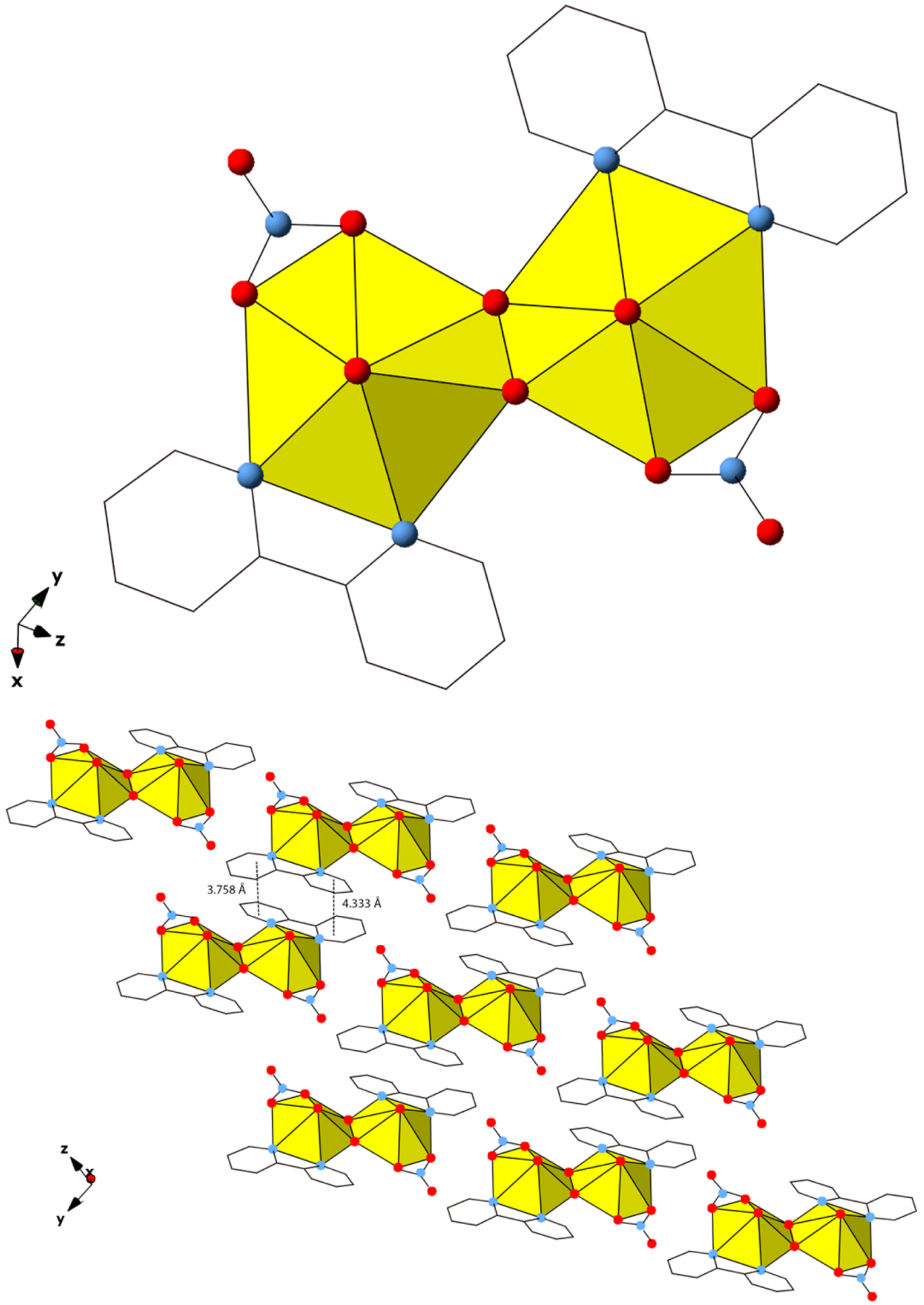

Figure 4. Top: The local structure of **1n** $[(UO_2)_2(NO_3)_2(O_2)(C_{10}H_8N_2)]$. Bottom: The packing diagram of **1n** (redrawn from ref 25).

between adjacent complexes are nearly identical, thus generating sheets in the (100) plane (Figure 8). In sum, the crystal structures and packing of **2** and **2n** are similar, but significant differences in the $U-O_2-U$ dihedral angles are observed based on the presence of acetate or nitrate ligands.

Crystal Structure of $[(UO_2)_3(CH_3COO)_4(O_2)(C_{15}H_{11}N_3)_2]$ (**3**). The structure of **3** contains three crystallographically unique uranyl cations (U1, O2 O3; U2, O6, O7; and U3, O13, O14) as seen in Figure 9. U1 is bound by one tridentate TPY via N1 (2.644(8) Å), N2 (2.623(8) Å), and N3 (2.594(7) Å), a monodentate acetate via O1 (2.372(6) Å), and a bidentate peroxide O4 (2.307(6) Å) and O5 (2.304(7) Å) (O4−O5 1.471(8) Å) to result in a hexagonal bipyramidal building unit. U2 is bound by two bidentate acetate ions via O8, O9, O10, and O11 ($U-O_{av}$, 2.473 Å) and a bidentate peroxide via O4 and O5 to result in a hexagonal bipyramidal building unit. U3 is

DOI: 10.1021/ic502767k
Inorg. Chem. 2015, 54, 4208−4221

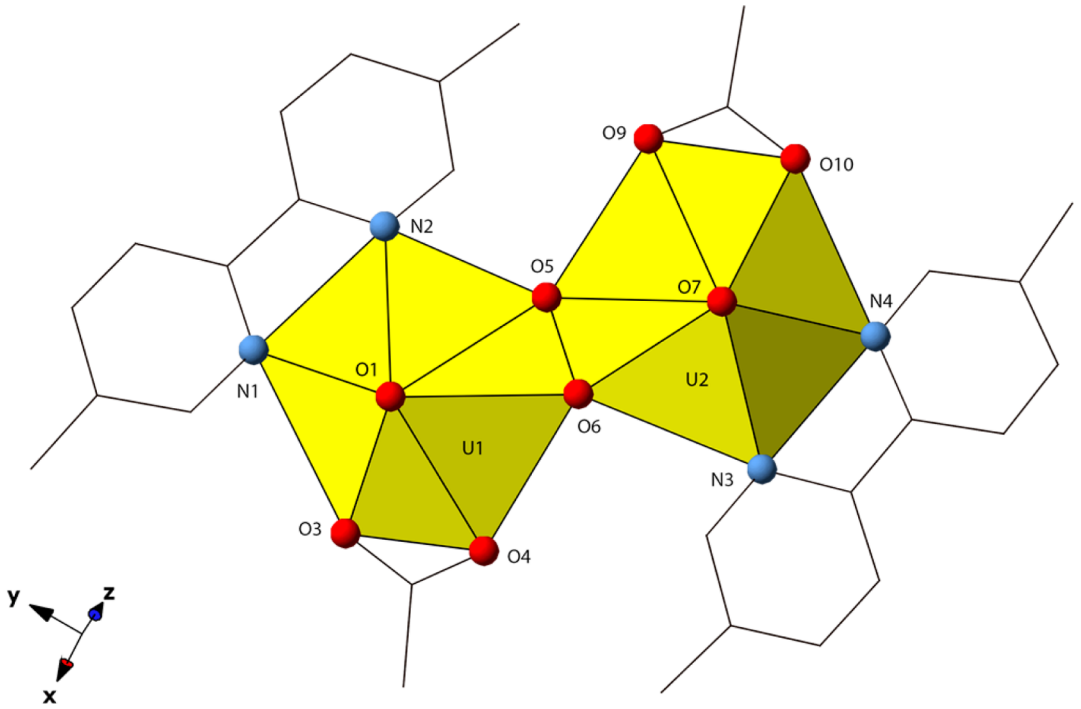

Figure 5. Local structure of **2**.

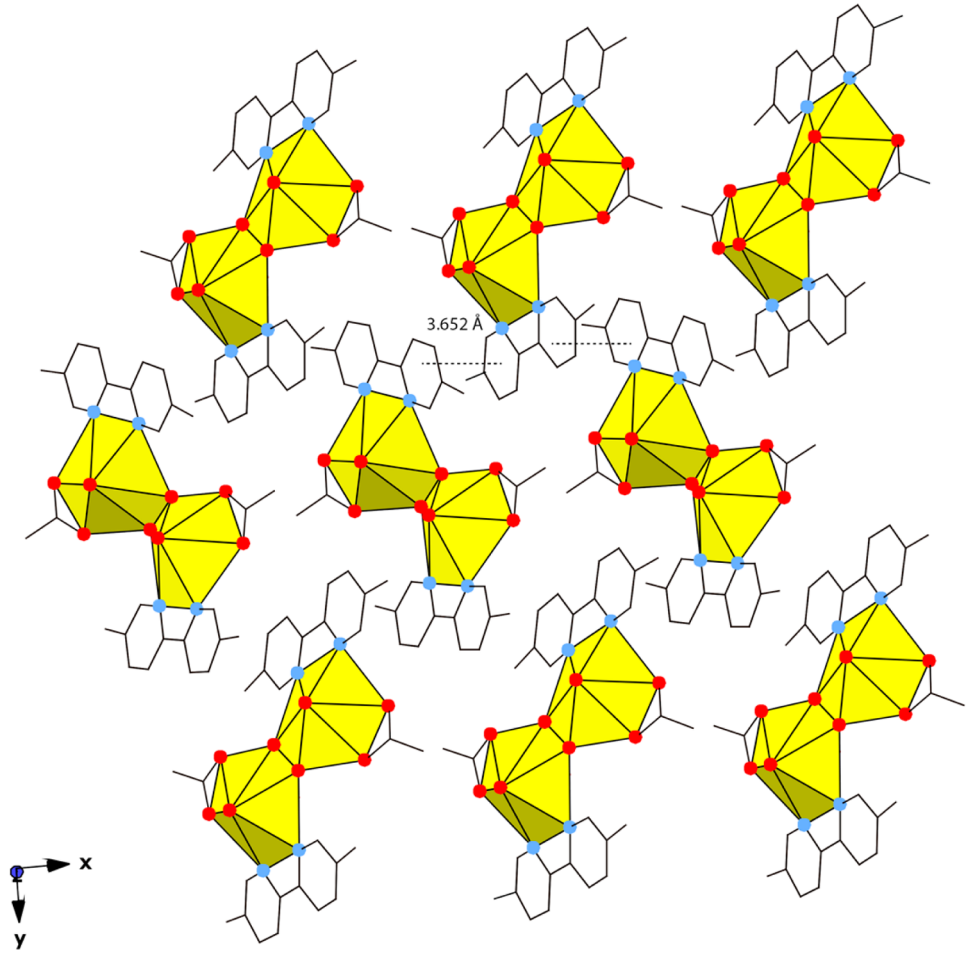

Figure 6. Packing diagram of **2**. $\pi-\pi$ interactions are shown as dashed lines.

DOI: 10.1021/ic502767k
Inorg. Chem. 2015, 54, 4208−4221

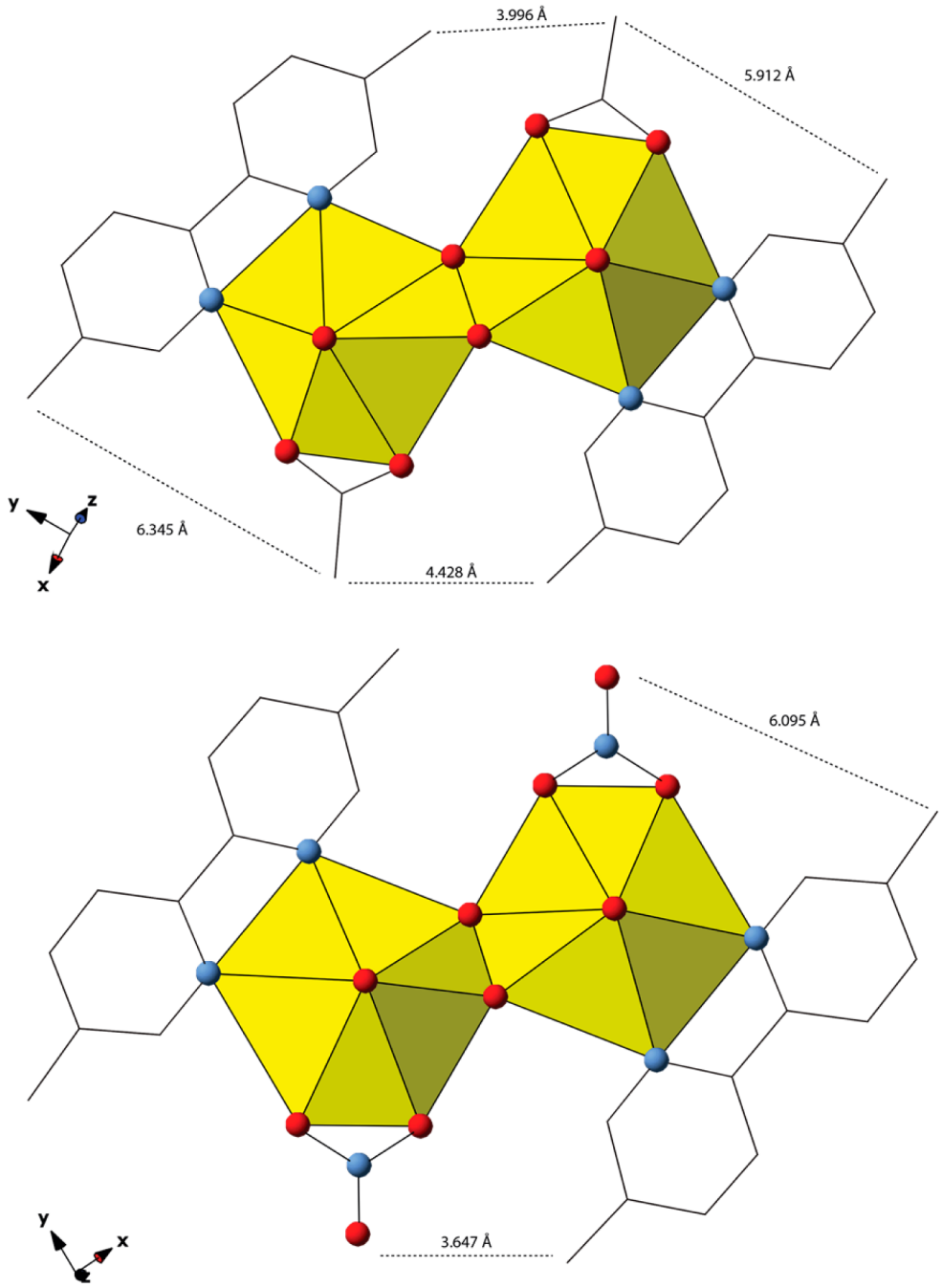

Figure 7. Comparison of measured distances in **2** and its nitrate analogue **2n** $[(UO_2)_2(NO_3)(O_2)(C_{12}H_{12}N_2)]$ (redrawn from ref 30).

bound by one tridentate TPY via N4 (2.573(9) Å), N5 (2.550(1) Å), and N6 (2.509(8) Å) and two monodentate acetate ions via O12 (2.337(6) Å) and O15 (2.210(1) Å) to result in a pentagonal bipyramidal building unit. U1 and U2 edge-share via the peroxide ion to result in the now familiar $[(UO_2)_2(O_2)]$ dimeric secondary building unit. This dimer is further connected to U3 via a bridging bidentate acetate ion to result in a pseudo trimer. These molecular pseudotrimers interact with each other through $\pi-\pi$ interactions (ring centroid−centroid distance, 3.369(1) Å) between the TPY ligands to result in 1-D chains that propagate in [010] as seen in Figure 10. Upon closer inspection of **3**, the U1−O_2−U2 dihedral angle is 143°, which is notably smaller than the dihedral angles of 159° and 151° in **1** and **2**, respectively.

The U−O_2−U angles for **1**−**3** and related uranyl peroxide materials (following the same method of determination) were compared (Table 5). This table shows the U−O_2−U bond angles in the reported uranyl peroxo materials vary widely; thus a clear trend to rationalize their differences within these materials is unclear. Yet, within our compounds, the size of N-donor ligands appears to systematically influence the dihedral angle in **1**−**3**. As the N-donor ligand becomes larger from BPY < MeBPY < TPY, the dihedral angle of the U−O_2−U peroxo bridge becomes smaller from 159°, to 151°, to 143°, respectively. The steric contributions of the methyl groups in MeBPY and the introduction of an additional pyridyl ring with TPY appear to influence the uranyl peroxo bridge and the bond angle conformations within these complexes. An analogous

DOI: 10.1021/ic502767k
Inorg. Chem. 2015, 54, 4208−4221

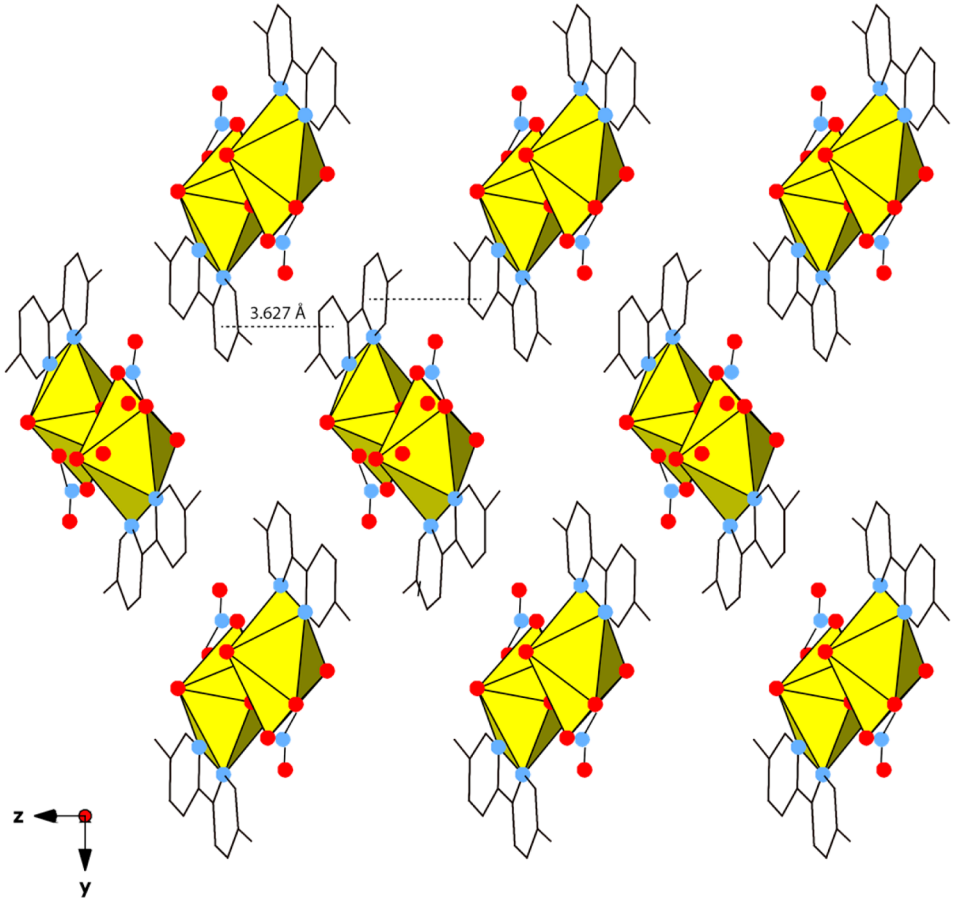

Figure 8. Packing diagram of **2n**, $[(UO_2)_2(NO_3)(O_2)(C_{12}H_{12}N_2)]$ (redrawn from ref 30).

steric argument was proposed by Burns and co-workers to describe possible reasons for the formation of differently sized uranyl peroxide nanoclusters.[41] The authors found that alkali metal cations of different size and electronegativity can tune the U−O_2−U dihedral angle and degree of curvature within these clusters, which consequently encouraged the formation of differently sized cage clusters.[42,43]

Discussion of Synthetic Routes and Mechanism of Peroxo Formation. The syntheses of **1**−**3** were carried out using either sunlight method A, heating method B, or sunlight/heating method B*, each of which resulted in crystals suitable for single-crystal XRD. Three uranyl complexes were observed and resulted in structures (**1**−**3**) that contain the acetate, BPY, MeBPY, and/or TPY ligands. In the synthetic protocols (methods A, B, B*), hydrogen peroxide was not used as an added reagent even though the peroxo ligand was observed in **1**−**3**. Compound **2** also formed in the presence of sunlight using method B*, which resulted in a more pure phase of **2** compared to methods A*, B, and B** (see Supporting Information Figures S2, S4, S5, and S8). In the absence of light (methods D and E), on addition of 30% H_2O_2, or by using solvothermal conditions, however, compounds **1**−**3** were not observed (see Supporting Information Figures S7−S14). We therefore believe that sunlight or (to a lesser extent) ambient light is required to promote in situ peroxo generation to form **1**−**3**. Moreover, carrying out the analogous sunlight method A for **1** in a Schlenk flask under nitrogen using anhydrous methanol and air-sensitive Schlenk techniques yielded no crystals or solids after 10 months of exposing the flask to sunlight. This result suggests that in addition to sunlight, atmospheric dioxygen is also required to promote in situ peroxo generation. These observations suggest a mechanism consistent with reported accounts of UO_2^{2+} photoexcitation in solutions.[16−18]

At this stage, it is perhaps worthwhile to introduce a more detailed treatment of the reaction mechanism reported by Bakac[19,20] and further adapted by Chen[21] to explain photodegradation of organic dyes. As such, Figure 11 is an overview of H_2O_2 formation from organic-containing systems via photoexcited UO_2^{2+}. The process begins with photoexcitation of ground-state UO_2^{2+} to form the $*UO_2^{2+}$ ion (step 1). This $*UO_2^{2+}$ species abstracts hydrogen from the organic substrate (in our case, methanol) to form an organic substrate radical intermediate (step 2). Here, the excited electron of $*UO_2^{2+}$ (from step 1) reduces a molecular O_2 species to form O_2^-. The O_2^- then reduces $*UO_2^{2+}$ to form the UO_2^+ intermediate (step 3). The organic radical intermediate (from step 2) reacts with molecular O_2 to produce the oxidized products, e.g., carboxylic acid and aldehyde (step 4). Subsequently, the UO_2^+ species (from step 3) is oxidized by molecular O_2 to form UO_2^{2+} (step 5). Further, H_2O_2 may also be produced as a result of a reaction between molecular O_2 and hydrogen ions (step 5). Moreover, Bakac suggested catalytic behavior as evidenced by regeneration of solution phase UO_2^{2+} and formation of excess H_2O_2.

With respect to peroxo formation in a *synthetic* context such as presented herein, assessing the exact mechanism as well as the potential for catalytic behavior is a bit more complex, especially when considering the presence of additional

DOI: 10.1021/ic502767k
Inorg. Chem. 2015, 54, 4208−4221

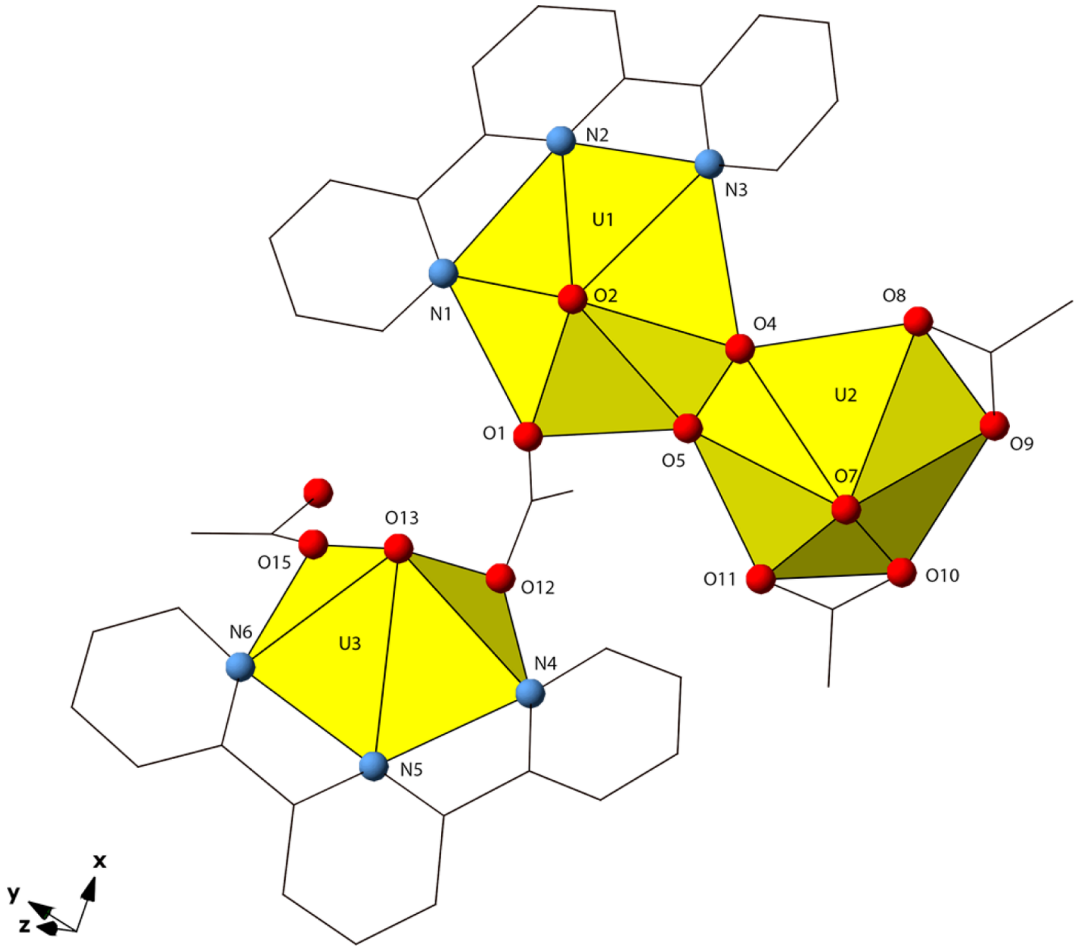

Figure 9. Local structure of **3**.

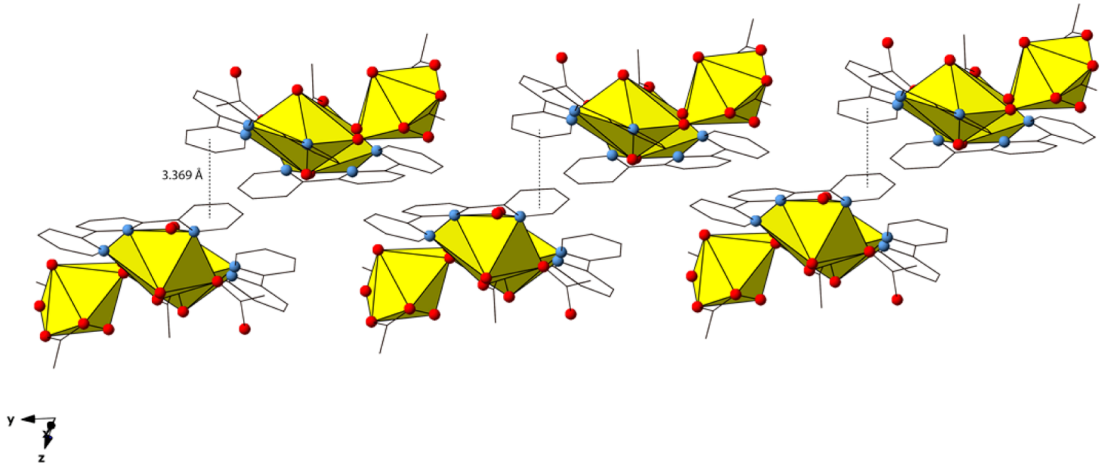

Figure 10. Packing diagram of **3** showing $\pi-\pi$ interactions of adjacent TPY uranyl centers.

(organic) chelating species such as BPY and TPY. That said, one indicator of the latter would be the formation of excess H_2O_2, which could be monitored via NMR.[44] Additionally, NMR may also provide mechanistic information via identification of oxidation products present in reaction mixtures. As such, a series of NMR experiments were conducted to investigate these possibilities.

In order to demonstrate that carboxylic acid and aldehyde products may also be generated by the oxidation of methanol by H_2O_2 (perhaps in conjunction with a reaction between the organic radical intermediate and molecular O_2 as shown in step 4 of Figure 11), an NMR spectrum of a 50% methanol/30% H_2O_2 (v/v) solution without UO_2^{2+} was obtained. The spectrum of this solution revealed H_2O_2 (~11.4 ppm) and peaks that may correspond to carboxylic acid and aldehyde (~9.9, 12.0 ppm; see Supporting Information Figure 33). This suggests the H_2O_2 oxidizes methanol to produce these species. For comparison, the NMR spectra of the supernatant methanol

DOI: 10.1021/ic502767k
Inorg. Chem. 2015, 54, 4208−4221

Table 5. U−O_2−U Dihedral Angles of Representative Uranyl Peroxide Materials

compound	U−O_2−U dihedral angle	ref
$Na_2Rb_4[(UO_2)_2(O_2)(C_2O_4)_4]$	153°	41
$[(UO_2)(O_2)(H_2O)_2{\cdot}2H_2O]$ (studtite)	140°	3
$[(UO_2)_2(CH_3COO)_2(O_2)(C_{10}H_8N_2)]$ (**1**)	159°	this work
$[(UO_2)_2(NO_3)_2(O_2)(C_{10}H_8N_2)]$	180°	25
$[(UO_2)(C_6H_5CO_2)(O_2)(C_{10}H_8N_2)]$	180°	26
$[(UO_2)_2(NO_3)(O_2)(C_{12}H_{12}N_2)]$	180°	30
$[(UO_2)_2(CH_3COO)_2(O_2)(C_{12}H_{12}N_2)]$ (**2**)	151°	this work
$[(UO_2)_2(CH_3COO)_2(O_2)(C_6H_5N)_2]{\cdot}C_6H_5N$	138°	24
$[(UO_2)_2(O_2)(C_4H_4O_4)(C_{10}H_8N_2)]$	148°	29
$[(UO_2)_3(CH_3COO)_4(O_2)(C_{15}H_{11}N_3)_2]$ (**3**)	143°	this work
$[(UO_2)_2(NO_3)_2(O_2)(C_6H_5N)_2]{\cdot}C_6H_5N$	125°	24

solutions of **1** and **3** (after exposure to sunlight for 7 days) were also obtained, yet no protons corresponding to H_2O_2 were observed. Peaks at approximately 9−10.0 and 12.0 ppm, corresponding to an aldehyde and carboxylic acid, were in fact observed (see Supporting Information Figures S31−S32) and suggest that any H_2O_2 produced has been consumed during methanol oxidation or in the formation of peroxo species that ultimately coordinate to UO_2^{2+}.

The absence of H_2O_2 in the supernatant is perhaps not surprising considering the affinity of the peroxo anion for UO_2^{2+} and subsequent precipitation of **1**−**3** (step 6, Figure 11). Moreover, this absence is perhaps an argument against catalytic behavior by UO_2^{2+}, as there is no excess, yet one must of course consider that any excess H_2O_2 produced could in fact be consumed in subsequent oxidations of methanol (such as a Baeyer−Villiger reaction[45]). The observation of aldehyde and carboxylic acid species, presumably from further oxidation of any radical intermediates post H abstraction (steps 1−4, Figure 11), is in fact anticipated, and the presence thereof is consistent with the mechanism outlined in Figure 11. One may also speculate that these oxidized products are the result of methanol oxidation by H_2O_2 regenerated after release from **1**−**3** (see dashed line, Figure 11). Again, considering the stability of these phases, we feel this is unlikely.

The syntheses of nitrate analogues **1n** and **2n** were also attempted using uranyl nitrate hexahydrate ($UO_2(NO_3)_2{\cdot}6H_2O$, 35 mg, 0.070 mmol, 1 equiv) and our synthetic methods A, B, and B*. The sunlight method A did not produce **1n** after 1 week of exposing uranyl methanolic solutions to sunlight, but crystals of **2n** were observed using heating/sunlight method B* only (see Supporting Information Figure S17). It is unclear why heating method B did not produce **2n** under ambient light, but it may be possible that a combination of both sunlight and ambient light (method B*) promotes in situ peroxo generation more effectively than ambient light alone in this system.

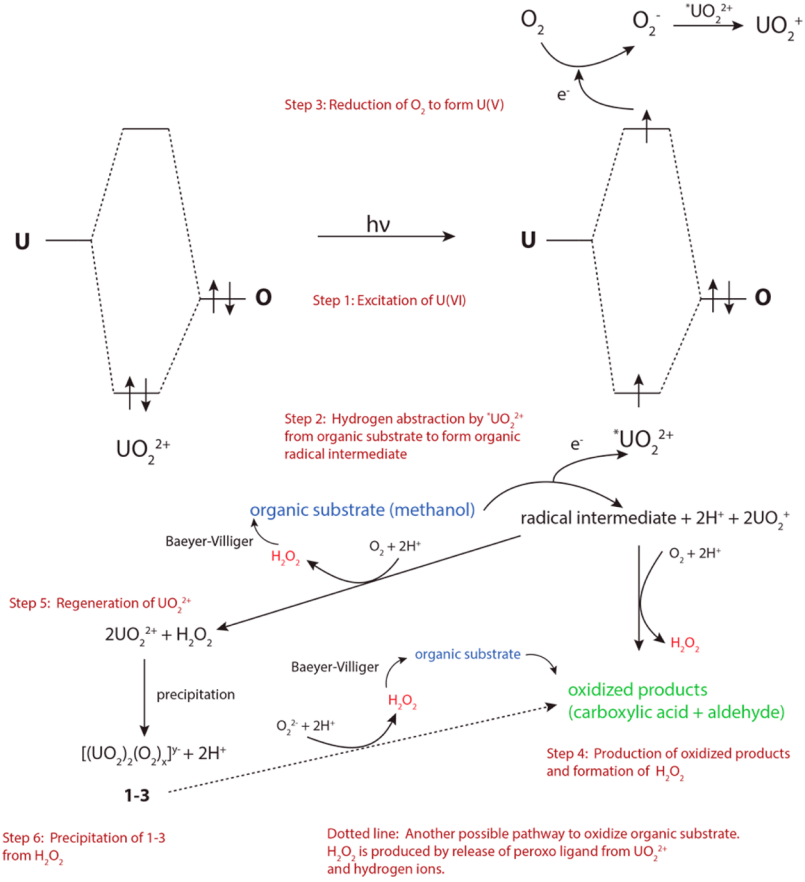

Figure 11. Proposed reaction mechanism for the degradation of organic substrates and subsequent formation of H_2O_2 via photoexcitation of UO_2^{2+} (steps 1−5) as inspired by Bakac et al.[19,20] and Chen et al.[21] Step 6 is the precipitation of **1**−**3**. A dotted arrow represents a potential (though less likely) process wherein O_2^{2-} released from **1**−**3** reacts with H^+ ions to produce H_2O_2 and subsequently oxidizes the organic substrate.

DOI: 10.1021/ic502767k
Inorg. Chem. 2015, 54, 4208−4221

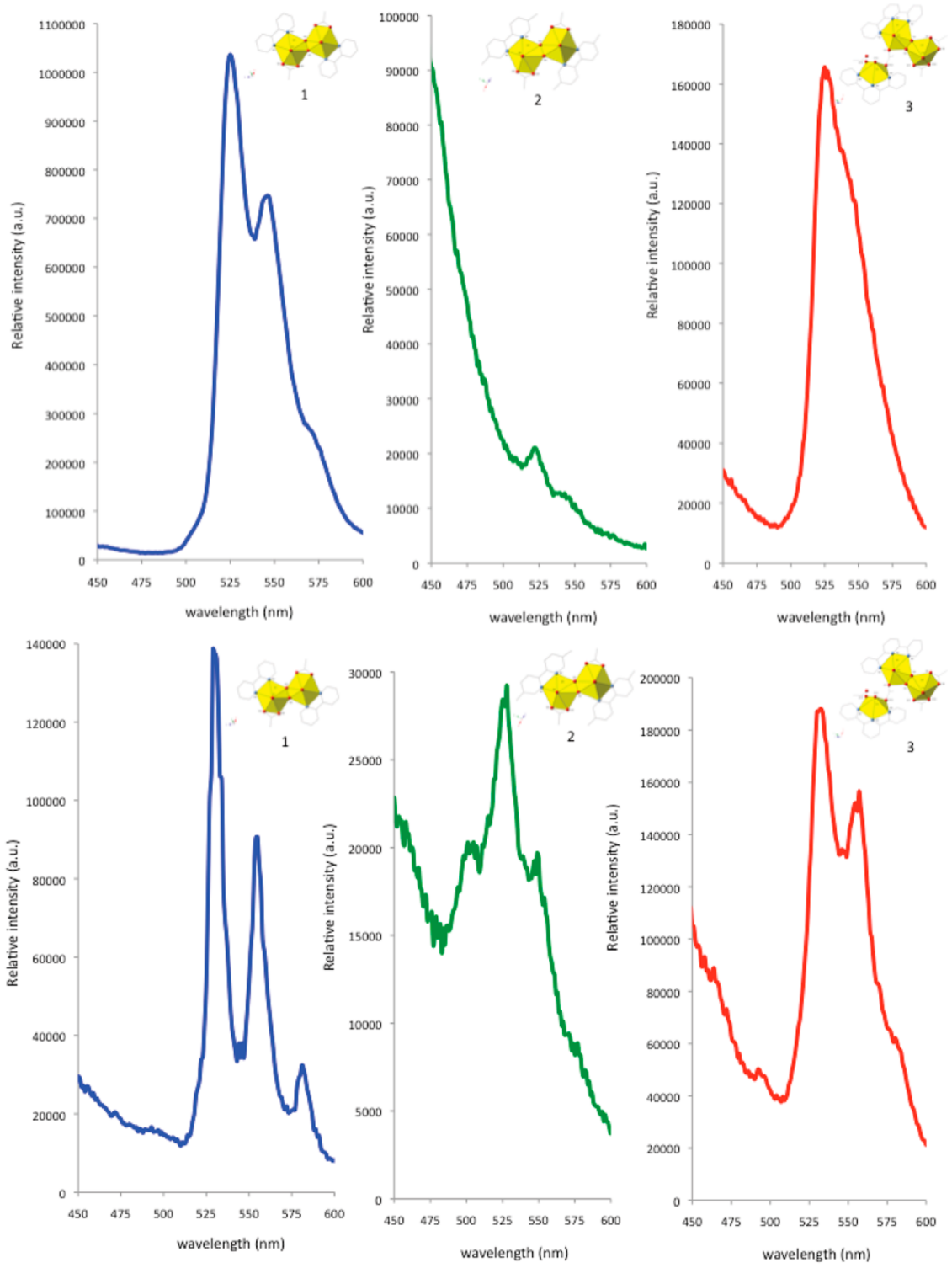

Figure 12. Solid-state emission spectra of **1**−**3** collected at 298 K (top) and 77 K (bottom) with an excitation wavelength of 365 nm.

Luminescence Studies. The emissive properties of the UO_2^{2+} cation have been well documented and can be used as a sensitive probe of the electronic structure of the uranyl unit itself.[46] UO_2^{2+} typically exhibits green emission between 470 and 590 nm consisting of five or six distinct vibronic peaks.[47] The vibronic structure of UO_2^{2+} emission stems from a strong coupling of the Raman-active symmetric (ν_1) oscillations of the U═O bond in the ground state with the electronic excited state.[48] A molecular orbital representation to explain UO_2^{2+} emission has been described in which relaxation of excited electrons from the LUMO 5f nonbonding orbitals to the HOMO σ-bond orbital is the principal cause for its spectral signature.[49]

Luminescence measurements of **1**−**3** were recorded at room temperature following excitation at 365 or 420 nm (Figure 12 and see Supporting Information Figure S24). Each complex shows a unique spectral signature, which does not resemble the reference spectrum of uranyl acetate (see Supporting

DOI: 10.1021/ic502767k
Inorg. Chem. 2015, 54, 4208−4221

Information S20). In compound **1**, the observed emission has a broad shape with two peaks at 525 nm (19 048 cm^{-1}) and 545 nm (18 349 cm^{-1}). The emission in **2** is very weak and poorly resolved as compared to **1**. Finally in **3**, the emission displays a single broad peak with a maximum centered at 526 nm (19 011 cm^{-1}). The observed features in **1**−**3** from 500 to 600 nm are nominally the axial oxygen ligand-to-metal charge transfer (LMCT) emissions within UO_2^{2+}. In all three cases, a broad featureless emission at higher energy (below ∼500 nm) is observed, and it is likely to originate from an additional competitive LMCT originating from equatorial ligands, either organic and/or peroxo[14,46,50−52] (see Supporting Information Figures S21−S23). Indeed, strong peroxo LMCT has been noted in other uranyl-peroxo compounds[14,52] and presented as a possible explanation for the loss of uranyl fine structure in the absorption spectra.

Additionally, luminescence measurements were recorded at low temperature (77 K; 365 nm excitation, Figure 12), wherein the spectra show enhanced resolution of the vibronic emission features. As the higher energy features (those below 500 nm) persist, it is thus difficult to conclude with certainty their origin.

In compound **1**, the observed low-temperature emission displays narrow vibronic peaks that are clearly resolved at 529 nm (18 904 cm^{-1}), 554 nm (18 050 cm^{-1}), and 581 nm (17 212 cm^{-1}). The measured differences between successive vibronic peaks are 854 and 838 cm^{-1} and are consistent with values for the Raman-active symmetric stretch of UO_2^{2+}.[53] Similarly, the emission profile of **3** (at 77 K) displays two vibronic peaks at 532 nm (18 797 cm^{-1}) and 556 nm (17 986 cm^{-1}). The difference between these peaks was measured to be 814 cm^{-1} and may also correspond to the Raman symmetric stretching frequency of UO_2^{2+}. A similar treatment for **2** was not attempted (even at low temperature) considering the poor resolution of the spectra. One may also note that interpretation of these values may be further complicated by additional coupling with the O−O symmetric stretch (878 cm^{-1}) of the peroxo ligand.[54] Finally, one must consider the number of potential influences on uranyl emission in materials like **1**−**3**. For example, $\pi-\pi$ interactions have been reported to enhance spectra,[33] whereas the influence of aromaticity has been shown to affect charge transfer between metal centers.[55−57] One should exercise some restraint when attempting a detailed interpretation of these spectra.

CONCLUSION

We have synthesized three novel uranyl-peroxo complexes containing the N-donor ligands BPY, MeBPY, and TPY (**1**−**3**). The presence of the peroxide ligand is due to in situ generation of hydrogen peroxide when the preparative solutions for **1**−**3** were exposed to heat and/or sunlight. We have proposed a formation mechanism consistent with those reported previously and suggest a noncatalytic pathway. In terms of structural features, The U−O_2−U bond angle observed in their crystal structures may be influenced by the size of the N-donor ligand, in which the angle becomes smaller as the size of the ligand becomes larger (i.e., BPY < MeBPY < TPY). Luminescence studies of **1**−**3** indicate that the uranyl emission profiles from these complexes may contain contributions from peroxo-based LMCT or residual ligand emission.

ASSOCIATED CONTENT

Supporting Information

CIFs of **1**−**3** at 298 and 77 K (CCDC 1026946−1026951), ORTEPs, PXRD patterns, and IR spectra. This material is available free of charge via the Internet at http://pubs.acs.org.

AUTHOR INFORMATION

Corresponding Author

*Phone: (202) 994-6959. E-mail: cahill@gwu.edu.

Notes

The authors declare no competing financial interest.

ACKNOWLEDGMENTS

This work was supported as part of the Materials Science of Actinides, an Energy Frontier Research Center, funded by the U.S. Department of Energy, Office of Basic Energy Science, under Award Number DE-SC0001089. We are grateful to Dr. Louise Natrajan (University of Manchester) for helpful comments regarding the luminescence data for **1**−**3**, as well as Drs. Adelina Voutchkova-Kostal and Arturo Azua Barrios (GW) for helpful discussions regarding the NMR experiments.

REFERENCES

(1) Qiu, J.; Burns, P. C. *Chem. Rev.* **2013**, *113*, 1097−1120.
(2) Zanonato, P. L.; Di Bernardo, P.; Grenthe, I. *Dalton Trans.* **2014**, *43*, 2378−2383.
(3) Burns, P. C.; Hughes, K.-A. *Am. Mineral.* **2003**, *88*, 1165−1168.
(4) Bühl, M.; Sieffert, N.; Wipff, G. *Dalton Trans.* **2014**, *43*, 11129−11137.
(5) Weck, P. F.; Kim, E.; Jove-Colon, C. F.; Sassani, D. C. *Dalton Trans.* **2012**, *41*, 9748−9752.
(6) Burns, P. C.; Kubatko, K.-A.; Sigmon, G.; Fryer, B. J.; Gagnon, J. E.; Antonio, M. R.; Soderholm, L. *Angew. Chem., Int. Ed.* **2005**, *44*, 2135−2139.
(7) Alcock, N. W. *J. Chem. Soc. A* **1968**, *1968*, 1588−1594.
(8) Zehnder, R. A.; Batista, E. R.; Scott, B. L.; Peper, S. M.; Goff, G. S.; Runde, W. H. *Radiochim. Acta* **2008**, *96*, 575−578.
(9) Kubatko, K.-A.; Forbes, T. Z.; Klingensmith, A. L.; Burns, P. C. *Inorg. Chem.* **2007**, *46*, 3657−3662.
(10) Nyman, M.; Rodriguez, M. A.; Campana, C. F. *Inorg. Chem.* **2013**, *49*, 7748−7755.
(11) Haegele, R.; Boeyens, J. C. A. *J. Chem. Soc., Dalton Trans.* **1977**, 648−650.
(12) Qiu, J.; Ling, J.; Jouffret, L.; Thomas, R.; Szymanowski, J. E. S.; Burns, P. C. *Chem. Sci.* **2014**, *5*, 303−310.
(13) Armstrong, C. R.; Nyman, M.; Shvareva, T.; Sigmon, G. E.; Burns, P. C.; Navrotsky, A. *Proc. Natl. Acad. Sci. U.S.A.* **2012**, *109*, 1847−1877.
(14) Adelani, P. O.; Ozga, M.; Wallace, C. M.; Qiu, J.; Szymanowski, J. E. S.; Sigmon, G. E.; Burns, P. C. *Inorg. Chem.* **2013**, *52*, 7673−7679.
(15) Rose, D.; Chang, Y.-D.; Chen, Q.; Zubieta, J. *Inorg. Chem.* **1994**, *33*, 5167−5168.
(16) Doyle, G. A.; Goodgame, D. M. L.; Sinden, A.; Williams, D. J. *J. Chem. Soc., Chem. Commun.* **1993**, *1993*, 1170−1172.
(17) Charpin, P. P.; Folcher, G.; Lance, M.; Nierlich, M.; Vigner, D. *Acta Crystallogr.* **1985**, *C41*, 1302−1305.
(18) Takao, K.; Ikeda, Y. *Acta Crystallograph. E* **2010**, *E66*, m539−m540.
(19) Nieweg, J. A.; Lemma, K.; Trewyn, B. G.; Lin, V. S. Y.; Bakac, A. *Inorg. Chem.* **2005**, *44*, 5641−5648.
(20) Wang, W.-D.; Bakac, A.; Espenson, J. H. *Inorg. Chem.* **1995**, *34*, 6034−6039.
(21) Wang, K.-X.; Chen, J.-S. *Acc. Chem. Res.* **2011**, *44*, 531−540.
(22) Yu, Z.-T.; Liao, Z.-L.; Jiang, Y.-S.; Li, G.-H.; Chen, J.-S. *Chem.—Eur. J.* **2005**, *11*, 2642−2650.

DOI: 10.1021/ic502767k
Inorg. Chem. 2015, 54, 4208−4221

(23) Xia, Y.; Wang, K.-X.; Chen, J.-S. *Inorg. Chem. Commun.* **2010**, *13*, 1542−1547.
(24) McGrail, B. T.; Pianowski, L. S.; Burns, P. C. *J. Am. Chem. Soc.* **2014**, *136*, 4797−4800.
(25) Charushnikova, I. A.; Den Auwer, C. *Russ. J. Coord. Chem.* **2004**, *30*, 511−519.
(26) Sokolova, M. N.; Bessonov, A. A.; Fedoseev, A. M. *Radiochemistry* **2012**, *54*, 341−345.
(27) Masci, B.; Thuéry, P. *Polyhedron* **2005**, *24*, 229−237.
(28) Alcock, N. W.; Flanders, D. J. *J. Chem. Soc., Dalton Trans.* **1985**, *1985*, 1001−1007.
(29) Wang, J.-L.; Deng, Z.-Y.; Duan, S.-B.; Xing, Y.-H. *J. Coord. Chem.* **2012**, *65*, 3546−3555.
(30) Akbarzadeh-T, N.; Kondori, T. *Res. Chem. Intermed.* **2013**, 1−8.
(31) Thangavelu, S. G.; Andrews, M. B.; Pope, S. J. A.; Cahill, C. L. *Inorg. Chem.* **2013**, *52*, 2060−2069.
(32) Yao, Y.; Odoh, S. O.; Thangavelu, S. G.; Gagliardi, L.; Cahill, C. L. *Unpublished results*.
(33) Harrowfield, J. M.; Lugan, N.; Shahverdizadeh, G. H.; Soudi, A. A.; Thuéry, P. *Eur. J. Inorg. Chem.* **2006**, *2006*, 389−396.
(34) Zucchi, G. l.; Maury, O.; Thuéry, P.; Gumy, F. d. r.; Bünzli, J.-C. G.; Ephritikhine, M. *Chem.—Eur. J.* **2009**, *15*, 9686−9696.
(35) Lhoste, J.; Henry, N.; Loiseau, T.; Guyot, Y.; Abraham, F. *Polyhedron* **2013**, *50*, 321−327.
(36) Sheldrick, G. *Acta Crystallogr. A* **2008**, *64*, 112−122.
(37) Farrugia, L. *J. Appl. Crystallogr.* **1999**, *32*, 837−838.
(38) Altomare, A.; Cascarano, G.; Giacovazzo, C.; Guagliardi, A. *J. Appl. Crystallogr.* **1993**, *26*, 343−350.
(39) Spek, A. L. *Acta Crystallogr.* **2009**, *D65*, 148−155.
(40) Bruno, I. J.; Cole, J. C.; Edgington, P. R.; Kessler, M.; Marcrae, C. F.; McCabe, P.; Pearson, J.; Taylor, R. *Acta Crystallogr. B* **2002**, *B58*, 389−397.
(41) Sigmon, G. E.; Ling, J.; Unruh, D. K.; Moore-Shay, L.; Ward, M.; Weaver, B.; Burns, P. C. *J. Am. Chem. Soc.* **2009**, *131*, 16648−16649.
(42) Vlaisavljevich, B.; Gagliardi, L.; Burns, P. C. *J. Am. Chem. Soc.* **2010**, *132*, 14503−14508.
(43) Miró, P.; Pierrefixe, S.; Gicquel, M.; Gil, A.; Bo, C. *J. Am. Chem. Soc.* **2010**, *132*, 17787−17794.
(44) Stephenson, N. A.; Bell, A. T. *Anal. Bioanal. Chem.* **2005**, *381*, 1289−1293.
(45) ten Brink, G. J.; Arends, I. W. C. E.; Sheldon, R. A. *Chem. Rev.* **2004**, *104*, 4105−4124.
(46) Redmond, M. P.; Cornet, S. M.; Woodall, S. D.; Whittaker, D.; Collison, D.; Helliwell, M.; Natrajan, L. S. *Dalton Trans.* **2011**, *40*, 3914−3926.
(47) Brachmann, A.; Geipel, G.; Bernhard, G.; Nitsche, H. *Radiochim. Acta* **2002**, *90*, 147−153.
(48) Liu, G. K.; Vikhnin, V. S. *Chem. Phys. Lett.* **2007**, *437*, 56−60.
(49) Denning, R. G. *J. Phys. Chem. A* **2007**, *111*, 4125−4143.
(50) Natrajan, L. S. *Coord. Chem. Rev.* **2012**, *256*, 1583−1603.
(51) Thuéry, P.; Harrowfield, J. *CrystEngComm* **2014**, *16*, 2996−3004.
(52) Goff, G. S.; Brodnax, L. F.; Cisneros, M. R.; Peper, S. M.; Field, S. E.; Scott, B. L.; Runde, W. H. *Inorg. Chem.* **2008**, *47*, 1984−1990.
(53) Cantos, P. M.; Jouffret, L. J.; Wilson, R. E.; Burns, P. C.; Cahill, C. L. *Inorg. Chem.* **2013**, *52*, 9487−9495.
(54) McGrail, B. T.; Sigmon, G. E.; Jouffret, L. J.; Andrews, C. R.; Burns, P. C. *Inorg. Chem.* **2014**, *53*, 1562−1569.
(55) Knope, K. E.; Cahill, C. L. *Inorg. Chem.* **2009**, *48*, 6845−6851.
(56) Kerr, A. T.; Cahill, C. L. *Cryst. Growth Des.* **2010**, *11*, 5634−5641.
(57) Kerr, A. T.; Cahill, C. L. *Cryst. Growth Des.* **2014**, *14*, 4094−4103.

DOI: 10.1021/ic502767k
Inorg. Chem. 2015, 54, 4208−4221